IEEE Access
Multidisciplinary | Rapid Review | Open Access Journal

Received 27 June 2022, accepted 17 July 2022, date of publication 20 July 2022, date of current version 25 July 2022.

Digital Object Identifier 10.1109/ACCESS.2022.3192528

RESEARCH ARTICLE

Numerical Studies on Antiresonant Waveguide Assisted Metasurface and Its Application

HYUNTAI KIM
Electrical and Electronic Convergence Department, Hongik University, Sejong 30016, Republic of Korea
e-mail: hyuntai@hongik.ac.kr

This work was supported by the National Research Foundation of Korea (NRF) grant funded by the Korea government under Grant 2021R1F1A1052193; and in part by the 2022 Hongik University Research Fund.

ABSTRACT The growth of the nanotechnology and intense studies on subwavelength nanophotonics has facilitated research in the field of metamaterials and metasurfaces. Optical waveguides has been a proper platform for metasurface applications because of its versatility and numerous infrastructure. In this paper, a metasurface interconnection method via attaching antiresonant waveguide is introduced. The antiresonant waveguide allows all-waveguide type inline metasurface schematic. Numerical calculations verified that the antiresonant fiber is capable of metasurface interconnection. In addition, an inline optical transmission modulator has been proposed by filling liquid crystal inside the hollow region. A liquid crystal device with on-state transmittance of 93.64%, and off-state transmittance of 0.96% with a smooth transient region are achieved.

INDEX TERMS Hollow waveguides, electromagnetic metamaterials, liquid crystal devices.

I. INTRODUCTION

Research on metamaterials and nanophotonics have accelerated as precise patterning is enabled due to the development of nano-processing technology. [1]–[3] In particular, metasurface, which applies nanostructures only to the surface, has great potential to be commercialized because of its ease of fabrication and its compact, thin size. [4]–[7] Various metasurfaces have been studied such as ultrathin lens, multi-focusing plate, super-resolution focusing oscillatory lens, and polarization-dependent optical component. [4], [8]–[11].

Optical waveguides, such as optical fibers or silicon waveguides, have been a great candidate as a metasurface platform. [12]–[16] By depositing metasurfaces at the core region of the waveguide facet, alignment problem between the light source and the metasurface is resolved. One can also choose a proper core size to control the beam size of the incident beam which interacts with the metasurface. [12], [16], [17] Moreover, the optical waveguide system is rich in infrastructure with various input/output equipment and devices.

In addition, hollow-core optical waveguide has also been introduced to be applied on metasurfaces. [18]–[20] After attaching a hollow-core optical waveguide over the metasurface, the waveguide protects the metasurface and guides the emitted light. When the metasurface is attached to a solid-core waveguide facet, the system becomes an all-fiberized or on-chip schematic, compatible with numerous optical fiber-based or silicon photonics-based devices. Various fluids can be introduced into the hollow area, which enables a higher level of surface protection or gas sensing. However, existing hollow-core waveguide-assisted metasurface research uses photonic bandgap fiber as a waveguide. Photonic bandgap hollow-core fiber generally is consisted of numerous sub-hollow regions, which is difficult to insert gas or fluid. The gas or fluid also fills the sub-hollow regions, which then affects the band characteristics of the periodic crystal. In addition, photonic bandgap design is difficult to be applied to silicon waveguides, limiting interconnection with metasurfaces fabricated on top of silicon substrates. Also, most of the previous studies used the hollow region only as a Fabry-Perot resonator, not to protect the metasurface or build an all-fiberized or all-silicon metamaterial system. In this research, antiresonant (AR) waveguide is introduced to be the interconnection waveguide from the metasurface. Compared to conventional photonic bandgap fibers, AR waveguide is applicable in both fiber optics and silicon photonics, so the metasurface interconnection via hollow-core

The associate editor coordinating the review of this manuscript and approving it for publication was Sukhdev Roy.

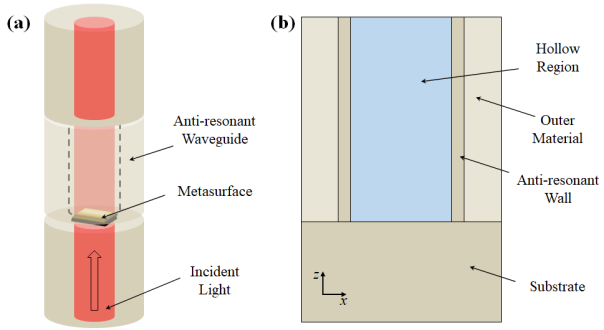

FIGURE 1. (a) Schematic of hollow-core waveguide protected metasurface. (b) 2-dimensional antiresonant waveguide structure.

waveguide is available on both schematics. [21]–[23] In addition, AR fiber has lower field-material interaction, which results in low loss and low nonlinearity. In addition, novel application based on metasurface-AR waveguide schematic is introduced. By depositing a polarizing metasurface on the both side of the AR waveguide interconnection surfaces and filling the hollow region with liquid crystal (LC), an optical device whose transmittance is controlled by voltage can be manufactured [24], [25]. The schematic is expected to be an electro-optic modulation device. The paper also suggests additional applications of AR waveguide-metasurface interconnected systems. The paper will first show the validity of the AR waveguide on solid surfaces via numerical calculations. Then metallic nanoslit – one of the simplest, but also which could be a core cell of metasurface – is combined to AR waveguide. Finally, the proposed LC based device is tested and optimized.

II. METHODS

The metasurface interconnection system via AR waveguide proposed in this paper is shown in Fig. 1(a). Various AR waveguides have already been proposed. In the case of optical fiber, there are tubular fiber, Kagome AR fiber, and nested AR nodeless fiber (NANF), etc., and for silicon type, there are Bragg waveguide and AR reflecting optical waveguide (ARROW) [21]–[23], [26]–[29]. The metasurface interconnection and protection method in this paper is compatible with all kinds of AR waveguides. Hereinafter, further discussion will be based on the most basic 2-dimensional AR waveguide. The shape of this 2-dimensional AR waveguide is shown in Fig. 1(b).

For further analysis, finite-element-method (FEM) based numerical simulations via COMSOL Multiphysics have been performed to analyze the characteristics of the AR waveguide connected metasurface schematic. The free-space wavelength is chosen as 1064 nm, which is a typical value for an ytterbium-doped fiber laser [30]. The material parameters of gold, silicon, silica and LC were taken from ref. [31]–[33], and [34], respectively. Perfectly matched layer covered the outer region to prevent unwanted reflection [35]. The finite element size has been chosen to be lower than $\lambda/7$, where λ is the wavelength within the material. Especially, for the case of lossy mediums such as metal has a higher imaginary refractive index than the real one, the larger value between real and imaginary components has been divided from the free-space wavelength. The effective wavelength in the material λ can be expressed as $\lambda_0/max(n_{material}, k_{material})$, where λ_0 is the free-space wavelength, $n_{material}$ and $k_{material}$ are real and imaginary refractive indexes of the material.

III. ANTIRESONANT WAVEGUIDE OPTIMIZATION

Even though the properties of the AR waveguide have been intensively studied previously, once more the transmittance is calculated by changing the thickness and internal material. It is assumed that light is incident from the silicon substrate, and the material of the thin wall is also assumed to be silicon. Since the thin wall is unstable if the inner region and outer region are both air or fluid, it is assumed that the outer wall is made of silica which has a lower refractive index compared to silicon. The internal material, which is the material of the hollow region, was assumed to be either air or LC. The core size, which is the width of the hollow region, was chosen to be 8 μ m, which is a typical core size for single-mode fibers. The incident light was set as a Gaussian beam with a beam waist of 2 μm. By calculating the transmission on different waveguide lengths, the transmission losses are calculated as shown in Fig. 2.

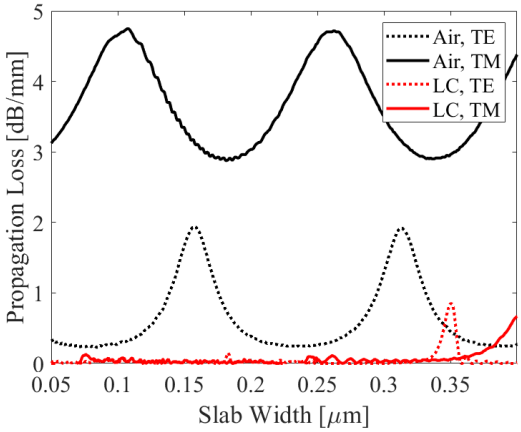

FIGURE 2. The propagation loss of 2-dimensional AR waveguide in terms of slab thickness depending on hollow region material and incident polarization.

When the refractive index of the inner material is less than the outer material, it is shown that the propagation loss is maximum at the resonance thickness as known. It is also already known that the transmittance varies considerably depending on the polarization of incident light – TM polarization suffers higher loss compared to TE polarization [21], [22]. When the index of the inner material is higher than that of the outer material, it is shown that there is almost no propagation loss, as the structure is similar to the step-index waveguide, except for the resonance thickness. However, it should be noted that the proposed system does

not require a long hollow region. Since only a certain length is required for protection, extremely low propagation loss is incidental. A few hundred micrometers or several millimeters of hollow-core waveguide are sufficient. If the hollow-core waveguide is to be used as the main transmission waveguides, photonic bandgap fiber, tubular fiber, or ARROW, etc. may be used instead of a 2-dimensional AR waveguide. The region of interest is 20 μm, therefore high propagation loss is not a critical issue. For application in further chapter, since both polarizations are used, a slab thickness of 0.186 μm is adopted to minimize propagation loss of TM polarization, which has a relatively large propagation loss.

IV. ANTIRESONANT WAVEGUIDE CONNECTED METALLIC NANOSLIT

Since polarizers are used in various optical systems, high-efficiency ultra-thin polarizer has great versatility. A metal nanoslit is a well-known type of polarizing plate, which transmits only one polarized light, can be explained based on the movement of electrons, effective medium theory, or surface plasmon polariton generation [4], [36]–[38]. Furthermore, the nanoslit array can be a unit cell of various metasurfaces. Although many studies have already investigated nanoslits, this study analyzes the nanoslit structures to confirm compatibility with AR waveguides and for optimization in further application. The proposed structure is shown in Fig. 3(a).

The substrate and the dielectric slab are assumed to be silicon, and the outer material has been assumed to be silica. Gold was chosen to be the metallic material. By iterating the metal thickness, period, duty ratio, the optical characteristics were calculated and optimized. In particular, calculations were carried out for the case where the fluid in the hollow region was air and LC, respectively. The length of the hollow-core waveguide has been assumed to be 5 μm. The AR waveguide parameters are identical as the optimized value in the previous section. As the substrate is assumed to be silicon, the reflection loss is significant due to the large index difference, so the control of thickness and duty ratio is important. If the effective index of the actual metallic region is the geometric average of the two regions, and the thickness exactly satisfies the anti-reflection thickness, the efficiency is maximized. The transmittance with respect to material and metal thickness for the case where other parameters are optimized – period of 100 nm and duty ratio of 0.49 for air and 0.34 for LC – is shown in Fig. 3(b). The label "Air, TE," for example, represents the case when the material of the hollow region is air and the incident polarization is TE mode.

The results show that the metallic nanoslit array prevents TE polarized light and transmits TM polarized light, and also show that the nanoslit structure is compatible with a hollow-core waveguide. As expected, it was confirmed that dielectric-like behavior was exhibited for TM polarized light and metal-like behavior was exhibited with respect to TE polarized light. When the medium was air, the nanoslit structure showed maximum transmittance of 85.5% when the thickness of the metal layer was 215 nm. For the case of

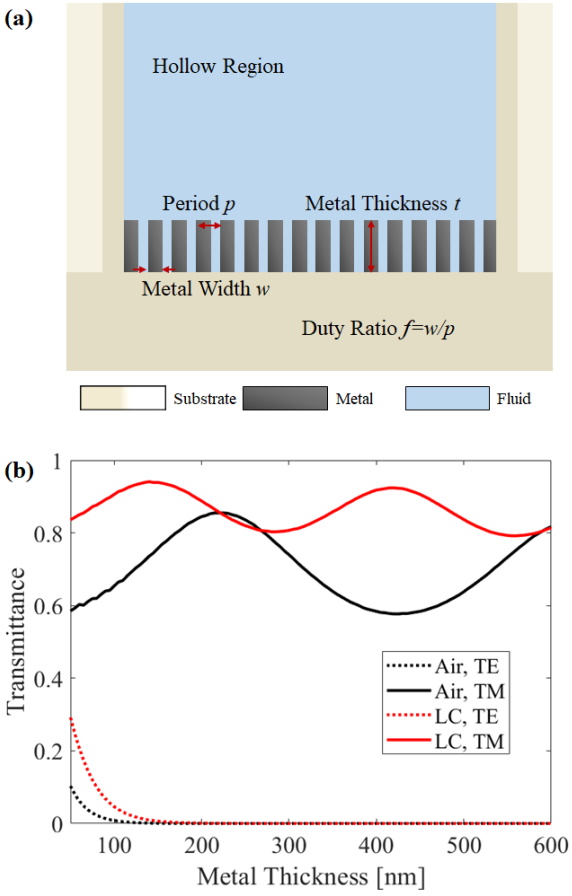

FIGURE 3. (a) Schematic of metallic nano-slit array polarizer protected by a hollow-core waveguide.(b) The transmittance of the metallic nanoslit in terms of metal thickness for TM and TE polarization while the medium of the hollow region is air and LC, respectively.

LC, the nanoslit structure showed maximum transmittance of 94.1% when the thickness of the metal layer was 140 nm. These optimized values are applied to nanoslit-based metasurface application in further discussion.

V. APPLICATION: INLINE LIQUID CRYSTAL ASSISTED TRANSMISSION MODULATOR

If a metamaterial polarizer can be implemented in the interconnection point between a solid substrate (or a solid-core waveguide) and an AR waveguide, an optical component in which polarizers are installed on both ends of the AR waveguide and filling the hollow region with LC can be considered. If the internal LCs are arranged in a twisted nematic structure, the proposed component can act as a waveguide inline metamaterial component similar to a liquid crystal display (LCD) cell which can control transmittance by tuning the voltage. (See Fig. 4) In a general twisted nematic structure, the azimuthal angle φ varies from 0 to $\pi/2$ depending on the transmission direction and the polar angle θ changes from $\pi/2$ to 0 as a function of applied voltage as depicted in Fig. 4(a). The proposed component, a LC-filled hollow-core waveguide

with pair of polarizers, is shown in Fig. 4(b). LC was chosen to be 4-pentyl-4'-cyanobiphenyl (5CB). The material parameter of LC was taken from ref. [34] at the wavelength of interest, 1064 nm, and an anisotropic relative permittivity tensor was applied for the simulations. The on-state voltage is assumed to be less than 5 V. [39] Note that the direction of polarizers on the top and at the bottom are the same (different from usual twisted nematic LCD panels) because the simulation is performed on 2-dimensional geometry. In the case of off-state without voltage, the polarization changes from TM to TE according to the orientation of twisted LC, so that the transmission becomes 0, such as shown in Fig. 4(c).

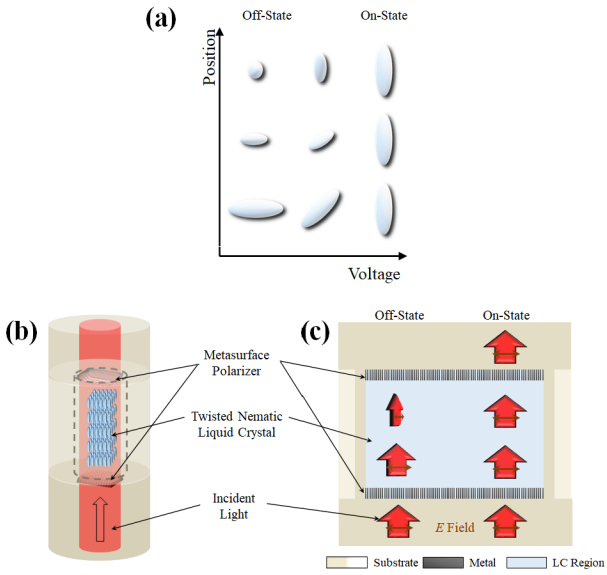

FIGURE 4. (a) The orientation of the twisted-nematic LCs in terms of position and voltage. (b) The schematic and (c) operation principle of LC-filled hollow-core waveguide with pair of polarizers.

In this cavity-like structure, resonance occurs according to the length of the hollow region. Since the refractive index of the propagation direction changes, the resonance condition varies according to the applied voltage, or the propagation direction refractive index n_z. Local maxima and minima appear under the following conditions.

$$l_{max} = \frac{m\lambda}{2n_z}, l_{min} = \frac{(m-\frac{1}{2})\lambda}{2n_z}, (m = 1, 2, \ldots) \quad (1)$$

where l_{max} and l_{min} are the hollow-region length where local maxima and local minima appear. Notably, the resonance condition of Eq. 1 is about the propagation direction, not the resonance at the dielectric slab for the AR waveguide. When the number of zeros between off-state and on-state is small, the transmittance to voltage function will show less fluctuation. However, if the length of the hollow region is too short, the polarization of light cannot be rotated properly while propagating, therefore allowing the incident light to be transmitted. Figure 5 shows the off-state transmittance calculated according to the length.

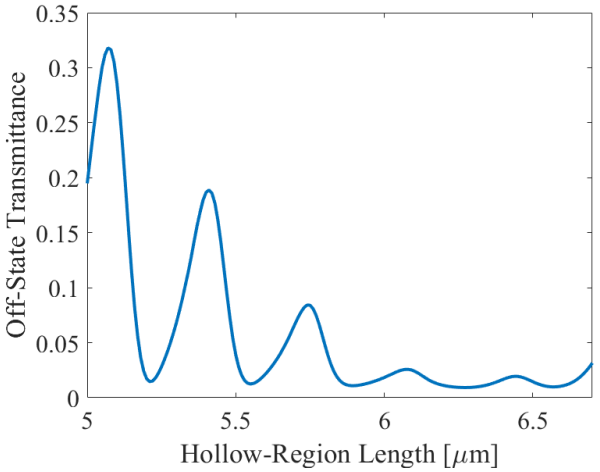

FIGURE 5. Transmittance at the off-state in terms of hollow-region length.

As shown in Fig. 5, when the length of the hollow region is less than 5.9 μm, the off-state transmittance fluctuates, showing high off-state transmission even at the local minima and with slight cavity length error will result in high off-state transmittance. So the length of the cavity should be at least 5.9 μm. The transmittance according to the polar angle and hollow-region length over the length is calculated and shown in Figure 6(a). The transmittance of each point with different cavity lengths and the polar angle of LC has been calculated via numerical simulations and depicted as a background colormap. The black solid line indicates the local minima computed by analytical calculations. Notably, the resonant state order m is depicted in Fig. 6(a). is 21, 22, and 23. For lower order resonant states, the electric field direction does not rotate fully as shown in Fig. 5.

In most cases, the relatively high transmittance of >90% in the on-state and low transmittance of <1% in the off-state is observed. The black solid line is the position of local minimums obtained by analytic calculation. Slight mismatch occurs due to phase change at the metallic nano-slit region and anisotropic refractive index distribution and polarization rotation, however, shows a considerably good match. There are several selection methods to choose the length of the cavity. If efficiency is important, a case with high on-state transmittance may be selected. Also, there are cases where the linearity of the transient region is required, or a small number of zeros are preferred. At a hollow region length of 6.3 μm, the on-state transmittance is 93.64%, and the off-state transmittance is 0.96%. In addition, the transient region shows a relatively smooth slope without zeros, as shown in Fig. 6(b). Figure 7 shows the full electric field intensity of the off-state and on-state where the length of the hollow region is 6.3 μm. Note that the polarization of the electric field is depicted as different orientations to express the rotation of the polarization. The vertical direction of the electric field represents the E_y component, where the vertical geometry represents z-direction. It is observed that the polarization has rotated

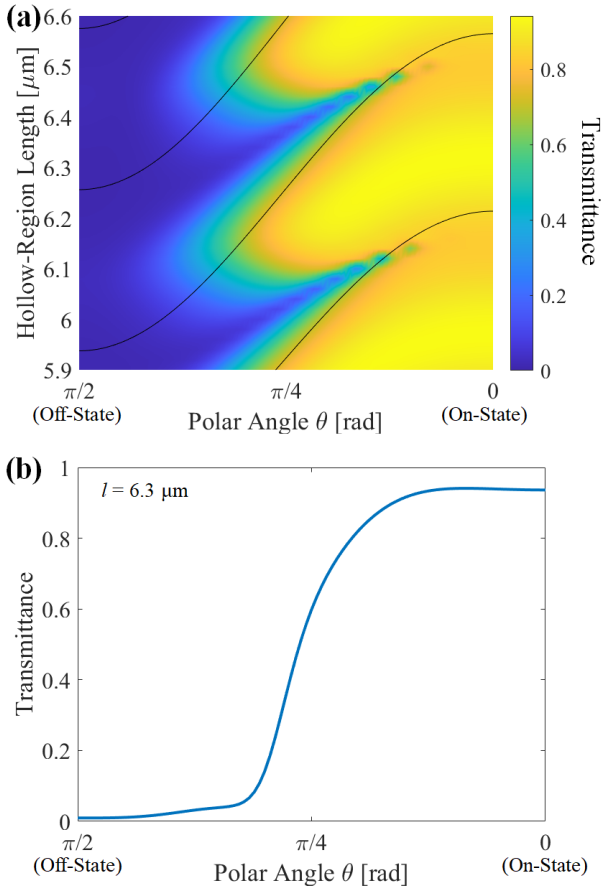

FIGURE 6. (a) The transmittance in terms of hollow-region length and polar angle. The black line indicates the local minima computed by analytical calculations. (b) The transmittance in terms and polar angle for particular cavity length.

$\pi/2$ at the off-state, which results in low transmission. On the other hand, the polarization is maintained without any rotation, allowing relatively high transmission. It is worth noting that oblique incident light is also available for AR waveguide and metasurface. However, the numerical aperture of the waveguide mode is low (<0.1) so the paper considered normal incidence light. In addition, higher-order modes are not considered, as the core size is a typical size of a single-mode fiber.

VI. DISCUSSION: FABRICATIONS AND FURTHER APPLICATIONS

As the paper is based on theoretical calculations and numerical simulations, fabrication methods and further applications are discussed in this chapter. Numerous studies exist to fabricate AR waveguides such as ARROW waveguide, tubular fiber, and NANF. [21]–[23], [26], [28], [29] Also, fabrication of metasurface based on electron beam lithography or focused ion beam has been studied and realized. [40]–[42] Here, the issue is to connect the metasurface and the AR waveguide. In order to align the metasurface exactly at the hollow region, the best method is to fabricate the metasurface at the

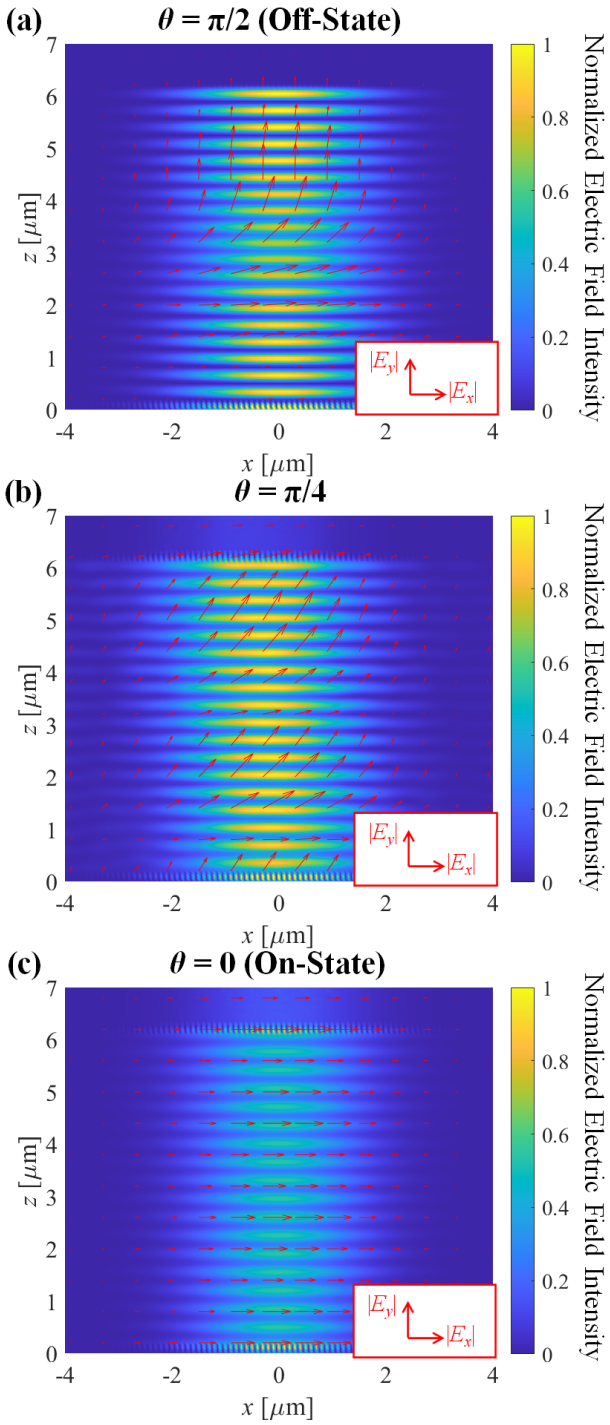

FIGURE 7. Calculated electric field intensity of the LC-filled optical component. The red arrow shows the electric field polarization of x-axis and y-axis.

center of a solid-core waveguide. [14]–[16] Methods such as heat splicing, laser splicing, or gluing two waveguides will complete the AR waveguide connected metasurface device. [19], [28] One may also first fabricate an ARROW type waveguide and then engrave the metasurface inside the desired region. The paper suggested one example of

application. However, metasurface-assisted AR waveguide schematic has numerous application potentials. One may think about a particle or an atom trapped in the hollow region. By attaching a metasurface lens at one or both sides of the hollow-core waveguide, optical trapping within the hollow region can be achieved, which would lead to an all-fiberized quantum physics experimental setup. [43]–[45] An active metasurface is capable to modulate the light inside the AR waveguide. [46], [47] A moth-eye structure or an anti-reflection metasurface layer could reduce the Fresnel reflection between the hollow region and solid region, reducing the insertion loss of the AR waveguide. [36], [48]

VII. CONCLUSION

An interconnection method between metasurface and AR waveguide was proposed. Compatibility between a metallic nano-slit array and an AR waveguide was checked and optimized. Furthermore, an optical component that can control transmission with voltage was proposed. Polarizers are placed on both ends after filling the hollow region with twisted nematic LC. The LC based device showed on-state transmittance of 93.64%, and off-state transmittance of 0.96% with a smooth transient region. The suggested method is applicable to various metasurfaces, and is expected to be used to produce various waveguide-inline metasurface schematics.

REFERENCES

[1] A. Q. Liu, W. M. Zhu, D. P. Tsai, and N. I. Zheludev, "Micromachined tunable metamaterials: A review," *J. Opt.*, vol. 14, no. 11, Nov. 2012, Art. no. 114009.
[2] G. Yuan, K. S. Rogers, E. T. F. Rogers, and N. I. Zheludev, "Far-field superoscillatory metamaterial superlens," *Phys. Rev. Appl.*, vol. 11, no. 6, Jun. 2019, Art. no. 064016.
[3] A. L. Rakhmanov, V. A. Yampol'skii, J. A. Fan, F. Capasso, and F. Nori, "Layered superconductors as negative-refractive-index metamaterials," *Phys. Rev. B, Condens. Matter*, vol. 81, no. 7, Feb. 2010, Art. no. 075101.
[4] D. Tang, C. Wang, Z. Zhao, Y. Wang, M. Pu, X. Li, P. Gao, and X. Luo, "Ultrabroadband superoscillatory lens composed by plasmonic metasurfaces for subdiffraction light focusing," *Laser Photon. Rev.*, vol. 9, no. 6, pp. 713–719, Nov. 2015.
[5] Z. Zhao, M. Pu, H. Gao, J. Jin, X. Li, X. Ma, Y. Wang, P. Gao, and X. Luo, "Multispectral optical metasurfaces enabled by achromatic phase transition," *Sci. Rep.*, vol. 5, no. 1, pp. 1–9, Dec. 2015.
[6] Y. Guo, Z. Zhang, M. Pu, Y. Huang, X. Li, X. Ma, M. Xu, and X. Luo, "Spoof plasmonic metasurfaces with catenary dispersion for two-dimensional wide-angle focusing and imaging," *iScience*, vol. 21, pp. 145–156, Nov. 2019.
[7] H.-T. Chen, A. J. Taylor, and N. Yu, "A review of metasurfaces: Physics and applications," *Rep. Prog. Phys.*, vol. 79, no. 7, 2016, Art. no. 076401.
[8] H. Ye, C.-W. Qiu, K. Huang, J. Teng, B. Luk'yanchuk, and S. P. Yeo, "Creation of a longitudinally polarized subwavelength hotspot with an ultra-thin planar lens: Vectorial Rayleigh–Sommerfeld method," *Laser Phys. Lett.*, vol. 10, no. 6, Jun. 2013, Art. no. 065004.
[9] X. Zang, H. Ding, Y. Intaravanne, L. Chen, Y. Peng, J. Xie, Q. Ke, A. V. Balakin, A. P. Shkurinov, X. Chen, Y. Zhu, and S. Zhuang, "A multi-foci metalens with polarization-rotated focal points," *Laser Photon. Rev.*, vol. 13, no. 12, 2019, Art. no. 1900182.
[10] H. Kim and E. T. F. Rogers, "Sub-wavelength annular-slit-assisted super-oscillatory lens for longitudinally-polarized super-resolution focusing," *Sci. Rep.*, vol. 10, no. 1, pp. 1–8, Dec. 2020.
[11] K. Chen, Y. Feng, Z. Yang, L. Cui, J. Zhao, B. Zhu, and T. Jiang, "Geometric phase coded metasurface: From polarization dependent directive electromagnetic wave scattering to diffusion-like scattering," *Sci. Rep.*, vol. 6, no. 1, pp. 1–10, Dec. 2016.
[12] H. Kim, J. Kim, H. An, Y. Lee, G.-Y. Lee, J. Na, K. Park, S. Lee, S.-Y. Lee, B. Lee, and Y. Jeong, "Metallic Fresnel zone plate implemented on an optical fiber facet for super-variable focusing of light," *Opt. Exp.*, vol. 25, no. 24, pp. 30290–30303, 2017.
[13] H. Kim, S.-Y. Lee, S. Koo, J. Kim, K. Park, D. Lee, L. A. Vazquez-Zuniga, N. Park, B. Lee, and Y. Jeong, "Theoretical study on the generation of a low-noise plasmonic hotspot by means of a trench-assisted circular nano-slit," *Opt. Exp.*, vol. 22, no. 22, pp. 26844–26853, 2014.
[14] W. Chen, W. Han, D. C. Abeysinghe, R. L. Nelson, and Q. Zhan, "Generating cylindrical vector beams with subwavelength concentric metallic gratings fabricated on optical fibers," *J. Opt.*, vol. 13, no. 1, Jan. 2011, Art. no. 015003.
[15] C. Guan, M. Ding, J. Shi, P. Hua, P. Wang, L. Yuan, and G. Brambilla, "Experimental observation and analysis of all-fiber plasmonic double airy beams," *Opt. Exp.*, vol. 22, no. 15, pp. 18365–18371, 2014.
[16] V. Savinov and N. I. Zheludev, "High-quality metamaterial dispersive grating on the facet of an optical fiber," *Appl. Phys. Lett.*, vol. 111, no. 9, Aug. 2017, Art. no. 091106.
[17] T. Phan, D. Sell, E. W. Wang, S. Doshay, K. Edee, J. Yang, and J. A. Fan, "High-efficiency, large-area, topology-optimized metasurfaces," *Light, Sci. Appl.*, vol. 8, no. 1, pp. 1–9, Dec. 2019.
[18] Y. Meng, Y. Chen, L. Lu, Y. Ding, A. Cusano, J. A. Fan, Q. Hu, K. Wang, Z. Xie, Z. Liu, Y. Yang, Q. Liu, M. Gong, Q. Xiao, S. Sun, M. Zhang, X. Yuan, and X. Ni, "Optical meta-waveguides for integrated photonics and beyond," *Light, Sci. Appl.*, vol. 10, no. 1, pp. 1–44, 2021.
[19] M. Ding, M. Komanec, D. Suslov, D. Dousek, S. Zvánovec, E. R. N. Fokoua, T. D. Bradley, F. Poletti, D. J. Richardson, and R. Slavík, "Long-length and thermally stable high-finesse Fabry–Pérot interferometers made of hollow core optical fiber," *J. Lightw. Technol.*, vol. 38, no. 8, pp. 2423–2427, Apr. 15, 2020.
[20] J. Flannery, R. Al Maruf, T. Yoon, and M. Bajcsy, "Fabry–Pérot cavity formed with dielectric metasurfaces in a hollow-core fiber," *ACS Photon.*, vol. 5, no. 2, pp. 337–341, Feb. 2018.
[21] W. Belardi and J. C. Knight, "Hollow antiresonant fibers with low bending loss," *Opt. Exp.*, vol. 22, no. 8, pp. 10091–10096, 2014.
[22] J. R. Hayes, S. R. Sandoghchi, T. D. Bradley, Z. Liu, R. Slavík, M. A. Gouveia, N. V. Wheeler, G. Jasion, Y. Chen, E. N. Fokoua, M. N. Petrovich, D. J. Richardson, and F. Poletti, "Antiresonant hollow core fiber with an octave spanning bandwidth for short haul data communications," *J. Lightw. Technol.*, vol. 35, no. 3, pp. 437–442, Feb. 2017.
[23] D. Yin, H. Schmidt, J. P. Barber, and A. R. Hawkins, "Integrated ARROW waveguides with hollow cores," *Opt. Exp.*, vol. 12, no. 12, pp. 2710–2715, 2004.
[24] M. Schadt and W. Helfrich, "Voltage-dependent optical activity of a twisted nematic liquid crystal," *Appl. Phys. Lett.*, vol. 18, no. 4, pp. 127–128, 1971.
[25] Y. Liu, C. Zhao, Y.-N. Zhang, G. Ma, X. Li, and Y. Zhao, "Electrically tunable optical fiber device based on hollow-core fiber infiltrated with liquid crystal," *Sens. Actuators A, Phys.*, vol. 318, Feb. 2021, Art. no. 112500.
[26] N. Wheeler, T. D. Bradley, J. R. Hayes, M. A. Gouveia, S. Liang, Y. Chen, S. R. Sandoghchi, S. M. Abokhamis Mousavi, F. Poletti, M. N. Petrovich, and D. J. Richardson, "Low-loss Kagome hollow-core fibers operating from the near-to the mid-IR," *Opt. Lett.*, vol. 42, no. 13, pp. 2571–2574, 2017.
[27] F. Poletti, "Nested antiresonant nodeless hollow core fiber," *Opt. Exp.*, vol. 22, no. 20, pp. 23807–23828, 2014.
[28] H. Sakr, T. D. Bradley, Y. Hong, G. T. Jasion, J. R. Hayes, H. Kim, I. A. Davidson, E. N. Fokoua, Y. Chen, K. R. H. Bottrill, N. Taengnoi, P. Petropoulos, D. J. Richardson, and F. Poletti, "Ultrawide bandwidth hollow core fiber for interband short reach data transmission," in *Proc. Opt. Fiber Commun. Conf.* Optical Society of America, Mar. 2019, pp. 1–3, Paper Th4A–1.
[29] P. Yeh, A. Yariv, and E. Marom, "Theory of Bragg fiber," *J. Opt. Soc. Amer.*, vol. 68, no. 9, pp. 1196–1201, Sep. 1978.
[30] Y. Jeong, S. Yoo, C. A. Codemard, J. Nilsson, J. K. Sahu, D. N. Payne, R. Horley, P. W. Turner, L. Hickey, A. Harker, M. Lovelady, and A. Piper, "Erbium: Ytterbium codoped large-core fiber laser with 297-W continuous-wave output power," *IEEE J. Sel. Topics Quantum Electron.*, vol. 13, no. 3, pp. 573–579, May/Jun. 2007.
[31] P. B. Johnson and R.-W. Christy, "Optical constants of the noble metals," *Phys. Rev. B, Condens. Matter*, vol. 6, no. 12, p. 4370, 1972.
[32] C. Schinke, P. C. Peest, J. Schmidt, R. Brendel, K. Bothe, M. R. Vogt, I. Kröger, S. Winter, A. Schirmacher, S. Lim, H. T. Nguyen, and D. MacDonald, "Uncertainty analysis for the coefficient of band-to-band absorption of crystalline silicon," *AIP Adv.*, vol. 5, no. 6, Jun. 2015, Art. no. 067168.

[33] I. H. Malitson, "Interspecimen comparison of the refractive index of fused silica," *J. Opt. Soc. Amer.*, vol. 55, no. 10, pp. 1205–1209, 1965.
[34] V. Tkachenko, G. Abbate, A. Marino, F. Vita, M. Giocondo, A. Mazzulla, F. Ciuchi, and L. D. Stefano, "Nematic liquid crystal optical dispersion in the visible-near infrared range," *Mol. Cryst. Liq. Cryst.*, vol. 454, no. 1, pp. 263–665, 2006.
[35] I. Ticar, O. Biro, and K. Preis, "A proof of the perfect matching property of PMLs in static fields," *IEEE Trans. Magn.*, vol. 35, no. 3, pp. 1139–1142, May 1999.
[36] H. Kim, "Metallic triangular pillar grating arrays for high transmission polarizers for air: Glass interfaces," *Jpn. J. Appl. Phys.*, vol. 58, no. 4, Apr. 2019, Art. no. 042001.
[37] F. Wang, M. Xiao, K. Sun, and Q.-H. Wei, "Generation of radially and azimuthally polarized light by optical transmission through concentric circular nanoslits in Ag films," *Opt. Exp.*, vol. 18, no. 1, pp. 63–71, Jan. 2010.
[38] H. Kim and S.-Y. Lee, "Optical phase properties of small numbers of nanoslits and an application for higher-efficiency Fresnel zone plates," *Current Opt. Photon.*, vol. 3, no. 4, pp. 285–291, 2019.
[39] M. Mrukiewicz, K. Kowiorski, P. Perkowski, R. Mazur, and M. Djas, "Threshold voltage decrease in a thermotropic nematic liquid crystal doped with graphene oxide flakes," *Beilstein J. Nanotechnol.*, vol. 10, no. 1, pp. 71–78, Jan. 2019.
[40] H. Lan and Y. Ding, *Nanoimprint Lithography*. Rijeka, Croatia: InTech, 2010.
[41] A. M. Korsunsky, E. Salvati, A. G. J. Lunt, T. Sui, M. Z. Mughal, R. Daniel, J. Keckes, E. Bemporad, and M. Sebastiani, "Nanoscale residual stress depth profiling by focused ion beam milling and eigenstrain analysis," *Mater. Des.*, vol. 145, pp. 55–64, May 2018.
[42] E. J. R. Vesseur, R. de Waele, H. J. Lezec, H. A. Atwater, F. J. G. de Abajo, and A. Polman, "Surface plasmon polariton modes in a single-crystal Au nanoresonator fabricated using focused-ion-beam milling," *Appl. Phys. Lett.*, vol. 92, no. 8, Feb. 2008, Art. no. 083110.
[43] O. M. Maragò, P. H. Jones, P. G. Gucciardi, G. Volpe, and A. C. Ferrari, "Optical trapping and manipulation of nanostructures," *Nature Nanotechnol.*, vol. 8, no. 11, pp. 807–819, Nov. 2013.
[44] D. Grass, J. Fesel, S. G. Hofer, N. Kiesel, and M. Aspelmeyer, "Optical trapping and control of nanoparticles inside evacuated hollow core photonic crystal fibers," *Appl. Phys. Lett.*, vol. 108, no. 22, May 2016, Art. no. 221103.
[45] T. H. Kim, "An optical-fiber interface to a trapped-ion quantum computer," Ph.D. dissertation, Massachusetts Inst. Technol., Cambridge, MA, USA, 2011.
[46] X. Yin, T. Steinle, L. Huang, T. Taubner, M. Wuttig, T. Zentgraf, and H. Giessen, "Beam switching and bifocal zoom lensing using active plasmonic metasurfaces," *Light, Sci. Appl.*, vol. 6, no. 7, Jul. 2017, Art. no. e17016.
[47] B. Gholipour, A. Karvounis, J. Yin, C. Soci, K. F. MacDonald, and N. I. Zheludev, "Phase-change-driven dielectric-plasmonic transitions in chalcogenide metasurfaces," *NPG Asia Mater.*, vol. 10, no. 6, pp. 533–539, Jun. 2018.
[48] C.-H. Sun, P. Jiang, and B. Jiang, "Broadband moth-eye antireflection coatings on silicon," *Appl. Phys. Lett.*, vol. 92, no. 6, Feb. 2008, Art. no. 061112.

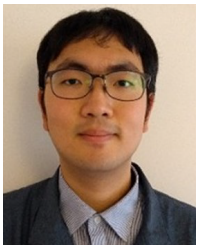

HYUNTAI KIM received the Ph.D. degree from the School of Electrical Engineering, Seoul National University (SNU), South Korea, in 2016. He was a Postdoctoral Fellowship at SNU, for one year. He joined the Optoelectronics Research Centre (ORC), University of Southampton, as a Research Fellow, in 2017. Since 2019, he has been a Faculty Member (Assistant Professor) with the Department of Electronic and Electrical Converged Engineering, Hongik University. His research interests include fiber optics and nanophotonics.